Localized Surface Plasmon Resonance on Optical Fiber Surface for Chemical Sensing

Amin Moslemi[1], Lucia Sansone[2][a], Flavio Esposito[1][b], Stefania Campopiano[1][c], Michele Giordano[2][d] and Agostino Iadicicco[1][e]

[1]Department of Engineering, University of Naples "Parthenope", 80143 Naples, Italy
[2]Institute for Polymers, Composites and Biomaterials, National Research Council of Italy, IPCB-CNR, 80055 Portici, Italy

Abstract: This study describes the basic principles of a fiber optic probe that exploits the localized surface plasmon resonance (LSPR) effect achieved by depositing gold nanoparticles (AuNPs) onto the fiber optic transducer. The idea is to read the absorbance spectra of AuNPs and its dependence on the environmental parameter, i.e. the surrounding refractive index, using optical fiber. Basically, we selected a thin optical fiber to encourage the presence of evanescent waves in the surrounding medium; furthermore, the fiber surface has been functionalized allowing the grafting of AuNPs while a silver mirror on the fiber tip allows readout for reflection configuration. The reflected spectra show absorbance characteristics related to single and aggregated AuNPs. In this article, the peaks absorbance, i.e. the depths of the reflected signal, were studied as a function of the surrounding refractive index for application in chemical sensing.

1 INTRODUCTION

The widespread adoption of optical fiber chemical and biological sensors is notable, offering significant potential to eventually supplant conventional and unwieldy sensing devices. Their compact size, flexibility, and resistance to electromagnetic interference make them promising candidates for future applications, facilitating remote measurements. These sensors find utility across diverse domains, including temperature, pressure, and refractive index (RI) monitoring, along with the quantification of biomarkers and chemical compounds (Choudhary et al., 2023; Esposito et al., 2021; Hernandez-Romano et al., 2015; Lu et al., 2022; Soares et al., 2021a).

Various optical detection techniques exist, necessitating diverse fiber geometries, materials, and equipment for implementation. Plasmonic approaches, such as surface plasmon resonance (SPR), stand out for their swift, label-free, and real-time sensitivity. In this mechanism, an interplay and energy exchange transpire between photons from incident light and electrons on a metal surface, resulting in their collective oscillation. SPR manifests at the interface between a dielectric and a metal nanofilm, leading to the propagation of surface plasmon polaritons (Esfahani Monfared, 2020; Mayer & Hafner, 2011; Sansone et al., 2021).

Gold nanoparticles (AuNPs) are favored for chemical and biosensor applications due to their distinct features, including excellent compatibility, intense light scattering/absorption, high surface area to volume ratios, selective interoperability through electrostatic interaction, stable structure, and non-toxicity (Huong et al., 2021; Jain et al., 2006; Saha et al., 2012; Zeng et al., 2011). Additionally, AuNPs are employed for the excitation of a unique phenomenon known as localized surface plasmon resonance (LSPR), extensively explored in recent sensing platforms due to its significant advantages (Chau et al., 2006; Do et al., 2020; Guerreiro et al., 2014).

[a] https://orcid.org/0000-0002-5032-6143
[b] https://orcid.org/0000-0003-1187-5825
[c] https://orcid.org/0000-0002-2987-9122
[d] https://orcid.org/0000-0003-0872-5578
[e] https://orcid.org/0000-0002-3540-7316

LSPR offers a compact, label-free, highly sensitive, and stable biosensing approach for detecting biological molecules (Wang et al., 2017; Willets & Van Duyne, 2007). This phenomenon in metallic nanostructures is associated with the resonance of free-electron waves in metal. Incident light can resonate with the oscillations of surface electrons at an excitation frequency, leading to the collective oscillation of surface plasmons, referred to as an LSPR mode (Unser et al., 2015).

In this paper, a fiber optic sensor is introduced for monitoring changes in the concentration of chemicals in a solution by measuring the refractive index. The proposed sensor is based on the deposition of gold nanoparticles around the fiber. The novelty in this study lies in utilizing both single and aggregated nanoparticle spectra to sense the surrounding refractive index area, supported by numerical results.

2 NUMERICAL RESULTS

In the numerical analysis, the Finite Element Method (FEM) is employed to simulate the interaction of light with AuNPs. At the core of this simulation lies either a single or an aggregate of nanoparticles, with a diameter of 50 nm for the single NP. Surrounding this central element is a 200 nm thick dielectric layer, and beyond that, another 200 nm dielectric layer acts as a Perfectly Match Layer (PML), as reported in Figure 1(a) whereas the zoom on the AuNP is highlighted in Figure 1(b).

The purpose of the PML is to establish an infinite dielectric environment around the gold structure. This configuration ensures that incident light is not reflected toward the gold structure, consequently minimizing the impact on the absorption band. The incoming light is planar in the z-direction, ranging from -z to +z, and polarized in the x-direction. The power of the illumination is maintained at 1 W/m².

Utilizing the FEM, the heat losses for each wavelength in VIS range are computed and subsequently plotted. This enables the plot of heat losses curve versus wavelength, i.e., the absorption spectrum. The red line in Figure 2 plots the absorption spectrum of a single 50 nm AuNP in water. According to (Lei et al., 2023; Litti & Meneghetti, 2019), 50 nm AuNP exhibits an absorption maximum at around $\lambda = 535$ nm. Interestingly, increase in AuNP size are manifested in slight redshift of the AuNPs absorption band. In the initial phase, the absorption spectrum of a single nanoparticle is investigated across various surrounding refractive indices (SRI) to determine sensitivity, as shown in Figure 2.
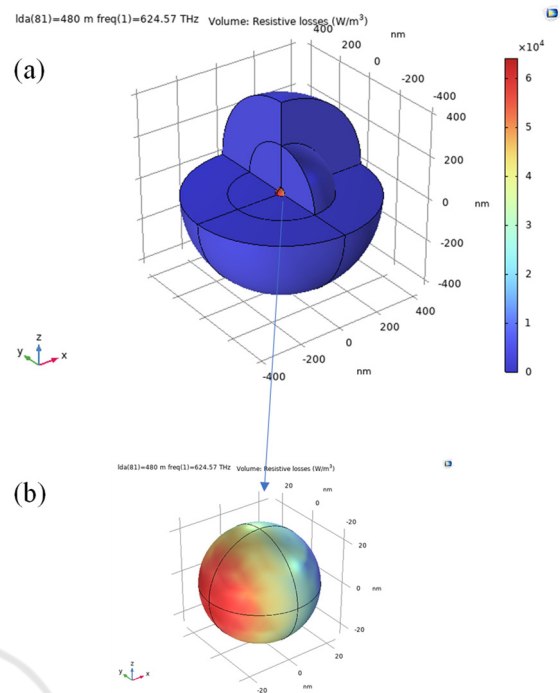

Figure 1: Schematic of the simulation environment: (a), various layers, encompassing the PML, dielectric layers, and the gold structure; (b) the electric field distribution around the individual gold nanoparticle.
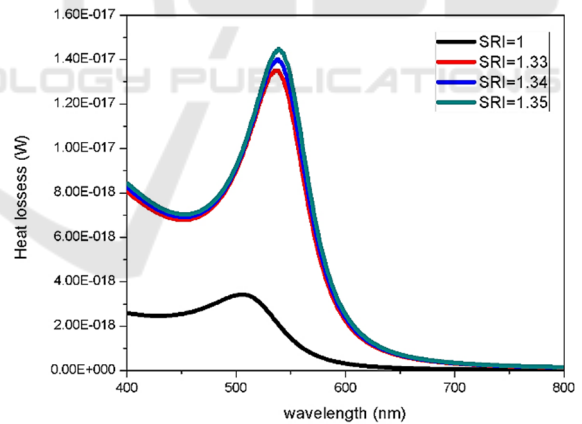
Figure 2: Absorption band of single AuNP in different environments: air, water, and a dielectric environment with refractive indices of 1.34 and 1.35.

Altering the refractive index of the surrounding medium induces a redshift in the absorption band peak. By tracking the resonance wavelength of this peak, as reported in Figure 3, the sensitivity of the system can be computed. This sensitivity value is determined to be around 200 nm/RIU (Refractive Index Unit, RIU).

Figure 3: Tracking of the resonance wavelength of the absorption band peak of a single gold nanoparticle across various surrounding refractive index values.

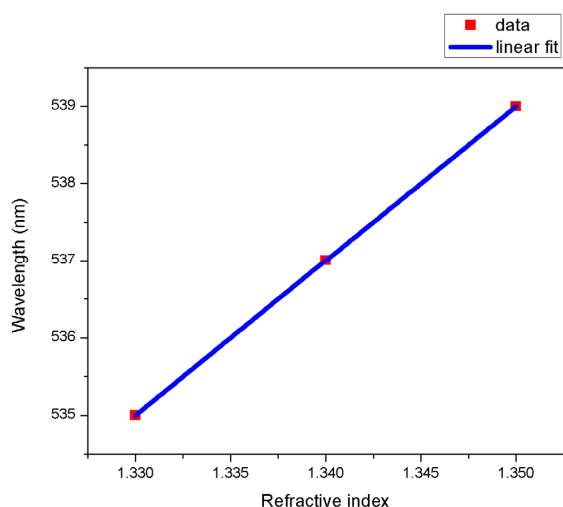The aim of the subsequent phase of the numerical simulation is the investigation of the effect of the aggregations. A full understanding demands various aggregation states to be explored. However, here, groups of 3 nanoparticles, each with a 50 nm diameter, are aggregated as reported in Figure 4, just as an example. The absorption band for each structure is then calculated. In a unique approach, each structure undergoes a 90° rotation around the x, y, and z axes during stimulation. Following this rotation, the superposition of all absorption spectra is computed. This step is essential, mirroring real-world scenarios where aggregated nanoparticles exhibit rotational dynamics.
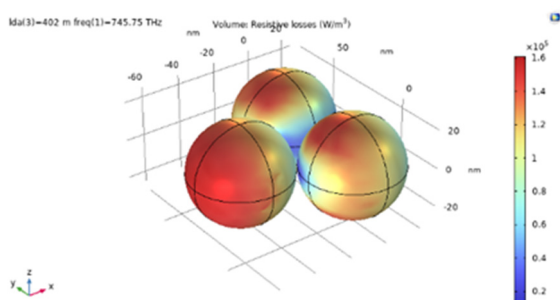

Figure 4: Distribution of absorption energy from incident light on the surface of three aggregated golden nanoparticles.

The resulting output spectrum is a superposition of numerous structures, incorporating different numbers of nanoparticles and incident angles. In Figure 5, the spectra of 3 nanoparticle group under various incident light angles are depicted, along with

their superposition. The superposition spectrum exhibits two mean resonance wavelengths at 560 nm and 678 nm, respectively. Although this analysis is not sufficient to investigate the state of all aggregations, we can retrieve that single AuNPs show an absorption peak around 520 nm whereas AuNPs aggregations, due to the larger size, show an absorption peak at a higher wavelength (Litti & Meneghetti, 2019).
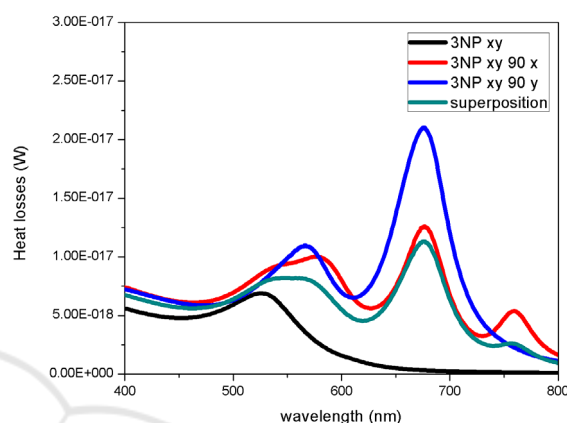

Figure 5: Absorption spectrum related to the superposition of different configurations involving 3 single nanoparticles.

3 MATERIALS AND METHODS

3.1 Chemicals

Tetrachloroauric acid ($HAuCl_4 \cdot 3H_2O$, 99%) and trisodium citrate (99%) were purchased from Merck Life Science (Milano, Italy), along with distilled water. Piranha solution (mixture of H_2SO_4 and H_2O_2 7:3 v/v). (3-Aminopropyl)triethoxysilane (APTES) in acetone (5% w/w).

3.2 AuNPs Preparation and Characterization

A solution containing 2.2 mM sodium citrate in distilled water (150 mL) was heated using a heating mantle in a 250 mL three-necked round-bottomed flask for 15 minutes under vigorous stirring. A condenser was employed to prevent solvent evaporation. Once boiling started, 1 mL of $HAuCl_4$ (25 mM) was injected. The solution colour transitioned from yellow to bluish-grey and then to a soft pink within 10 minutes. Immediately following the synthesis of the Au seeds and within the same reaction vessel, the reaction was cooled until the solution temperature reached 90 °C. Subsequently, 1

mL of a HAuCl$_4$ solution (25 mM) was injected. After 30 minutes, the reaction was concluded. This process was repeated twice. Subsequently, the sample was diluted by extracting 55 mL of the solution and adding 53 mL of MQ water and 2 mL of 60 mM sodium citrate. This resulting solution served as the seed solution, and the process was reiterated five times (Figure 6).
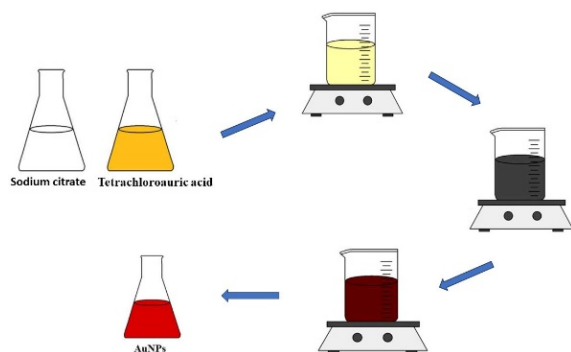

Figure 6: Synthesis of gold nanoparticles.

To examine the morphology of AuNPs, transmission electron microscopy (TEM) experiments were carried out using a TEM FEI Tecnai G12 Spirit Twin equipped with a LaB6 emission source (120 kV) and coupled with a CCD camera Fei Eagle 4K (Japan). For TEM specimen preparation, a drop of the diluted AuNPs suspension was deposited onto a carbon-coated copper grid. Subsequently, the sample was air-dried and loaded into the electron microscope chamber.

The mean size and distribution of the nanoparticles were determined through dynamic light scattering (DLS) analysis. The measurements were conducted at 25 °C using a Malvern DLS instrument (model Zetasizer Nano ZS90, Malvern Instruments Ltd., Worcestershire, UK), featuring a He-Ne laser source at 632.8 nm and a detector set at a scattering angle of 90°. Low-volume quartz batch cuvettes (model ZEN2112, Malvern Instruments Ltd., Worcestershire, UK) served as the sample cells.

UV-Vis absorption spectra of AuNPs were obtained using an Agilent Cary 60 UV/Vis spectrophotometer, employing quartz cuvettes. To prevent absorption saturation, dispersion samples were appropriately diluted in deionized water at a ratio of 1:8 v/v.

The two AuNPs water solutions were diluted at a ratio of 1:10 v/v, and their size and polydispersity index (PDI) were assessed through DLS analysis. The presence of a single peak was observed for the AuNPs solutions, corresponding to a size of 50.4 ± 5 nm (PDI = 0.019). Additionally, the low values of PDI indicate

the high quality and monodisperses of the AuNPs water solution. Figure 7 displays the visible (VIS) spectrum of AuNPs, revealing a plasmon resonance band at 535 nm. The narrow shape of the band suggests a high uniformity in particle sizes. According to (Bastús et al., 2011), the size of AuNPs is approximately 50 nm.
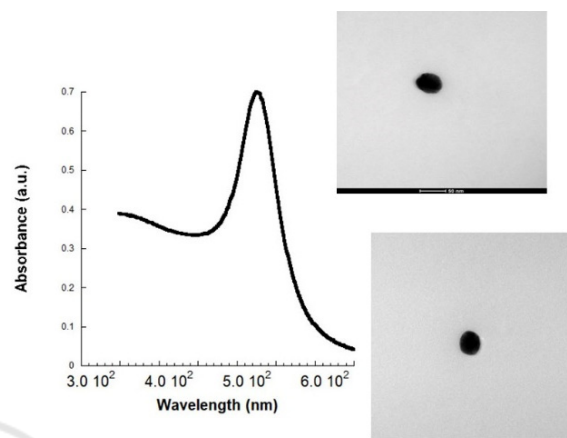

Figure 7: UV spectrum and SEM images of AuNPs 50 nm.

3.3 Optical Transducer

The functioning principle of this sensor is grounded in the response of 50 nm gold nanoparticles to chemicals, probed by a fibre optics transducer, as schematically reported in Figure 8.

The transducer incorporates a multimode fiber (MMF) with core/cladding size of 105/125 μm spliced with a short piece (less than 5 cm) of coating free glass thin fiber with diameter of 80 μm.

To design a simple probe and capture the reflection spectrum, the second end of the thin fiber is sharply cut and mirrored to enhance reflection power. Due to the fiber size mismatching, light in thin fiber exhibits evanescent waves interacting with surrounding medium.

Subsequently, nanoparticles are deposited around the thin fiber, revealing an attenuation band in the reflected spectrum of the device. Such attenuation band is located at those wavelengths for which the light is absorbed by the presence of nanoparticle, as illustrated in the simulation section. This spectrum changes in response to variations in the environment, influencing the electrical and optical properties of nanoparticles. Here, these changes are monitored to sense alterations in the surrounding area.
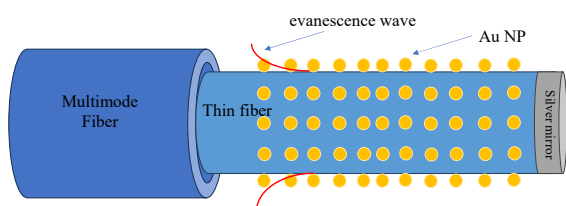
Figure 8: Schematic of Optical Transducer.

3.4 Experimental Setup

The optoelectronic readout experimental arrangement is shown in Figure 9 and comprises a broadband light source (Avantes AvaLight-HAL-S-Mini). The light is conveyed to the transducer using one branch of a multimode fiber coupler, and the resulting reflection spectrum is directed to a spectrometer (Ocean Optic HR2000+) via the second channel of the coupler.
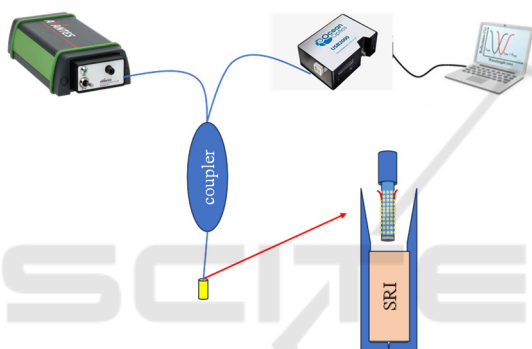

Figure 9: Schematic of the optoelectronic readout setup.

4 FABRICATION OF THE FIBER PROBE

The multimode fiber with 105/125 µm core/cladding diameter (FG105LCA Thorlabs) was fused with a 5 cm length of 80 µm thin fiber (SM1500(4.2/80) Fibercore). A microscope picture of the fibers is reported in Figure 10(a) and Figure 10(b), before and after the splicing, respectively. The free end of the multimode fiber was linked to the coupler. Then the second end of the thin fiber was sharply cleaved and mirrored using Tollen's reaction.

Figure 11 plots the spectra of the fiber device during the fabrication steps using the cleaved multimode fiber as reference. Consequently, the reflectance after coating the mirror exceeds 100% due to this factor. According to Figure 11, this resulted in an approximately fivefold increase in the amplitude of the reflection signal.

The subsequent step involved depositing nanoparticles onto the fiber. Given that neutral glass
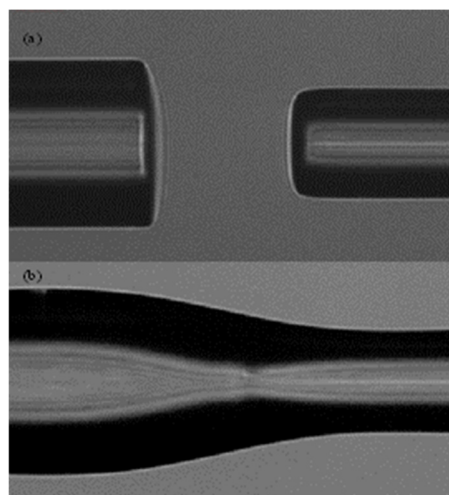

Figure 10: Microscope images: a) Multimode and thin fiber before splicing; b) The spliced area of the multimode fiber and thin fiber.
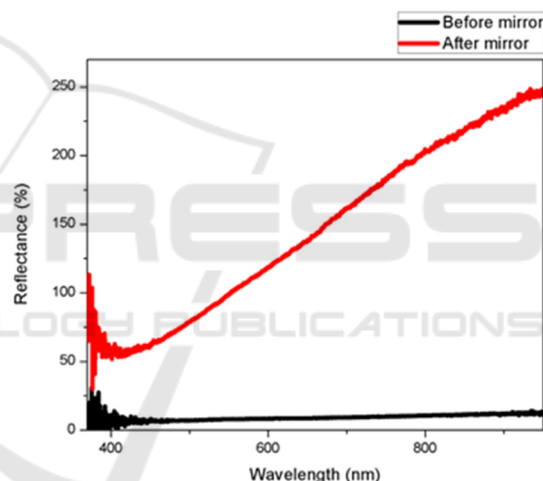

Figure 11: Reflection spectrum of the transducer before and after mirror.

is not inherently attractive to gold nanoparticles, it was essential to impart a positive charge to the glass surface through a surface functionalization. To achieve this, the thin fiber was immersed in a piranha solution (mixture of H_2SO_4 and H_2O_2) for one hour, subsequently washed with water. This procedure has been carried before mirror to avoid any damage due to the chemicals.

Following, the mirrored fiber was immersed in APTES (5% w/w) for two hours, washed with acetone, and allowed to air-dry overnight (Soares et al., 2021b; Sypabekova et al., 2022).

Subsequently, the fiber was immersed in the solution containing gold nanoparticles (50 nm, 1 mM) for 2.5 hours and left to dry overnight. Figure 12

illustrates the spectrum of the transducer after depositing gold nanoparticles, taken in the air using the mirrored fiber (red line of Figure 11) as reference. Here, two minima are well visible; based on the numerical section, we retrieve that the left one is related to single AuNPs whereas the wide attenuation peak at higher wavelength can be attributed to AuNPs aggregations.
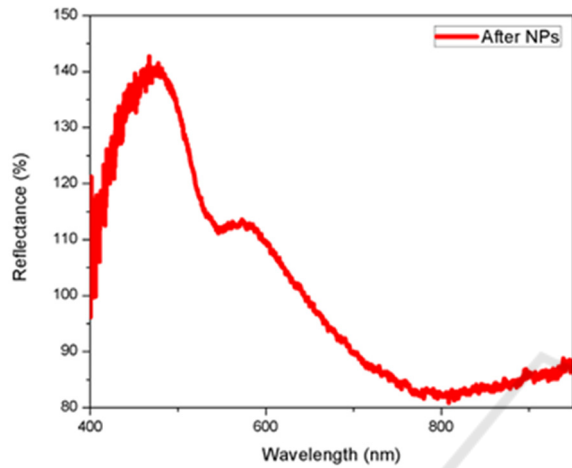
sensitivity of the second peak surpasses that of the first peak by more than fourfold.
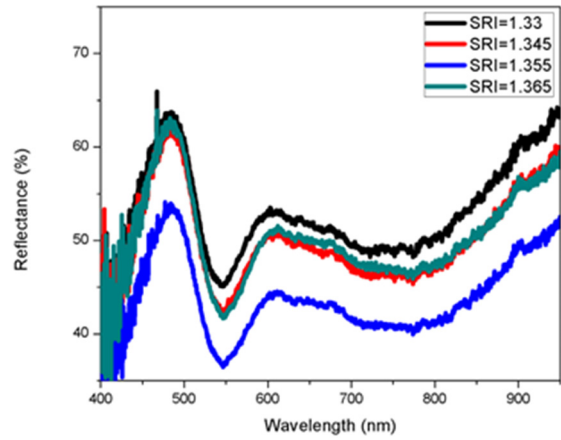
Figure 13: Reflection spectrum of the transducer in different surrounding area refractive indices.

Figure 12: Reflection spectrum of the transducer in air after depositing nanoparticles.

5 SENSING RESULTS

The sensor sensitivity was assessed through experimentation with the surrounding refractive index. In this evaluation, various solutions were prepared by blending deionized water and glycerine in different proportions. The precise refractive index of each solution was then determined using an Abbe refractometer.

Subsequently, the sensing area was fully immersed in each solution. The spectrum was recorded, and the fiber was extracted, sequentially immersed in deionized water to rinse off glycerine residues, air-dried briefly, and the process was repeated for subsequent solutions.

As one can observe in Figure 13, both the first and second peaks exhibited a redshift with an increase in the refractive index, which agrees well with numerical simulations.

For tracing the resonance wavelength of the minima, a second-order polynomial was fitted to each one, and then the minimum of each polynomial was traced. Figure 14 illustrates the shift of each minimum. The sensitivity of the first and second peaks was found to be around 90 nm/RIU and 450 nm/RIU, respectively. It is noteworthy that the

Figure 14: Resonance wavelength shift data and linear fit for the (a) first and (b) second minima, respectively.

6   CONCLUSIONS

In conclusion, this paper conducted simulations on various configurations of nanoparticle aggregation, calculating absorption bands for each scenario. Subsequently, a novel fiber optics probe was designed and fabricated, relying on the deposition of nanoparticles on the thin fiber surface. The key innovation lie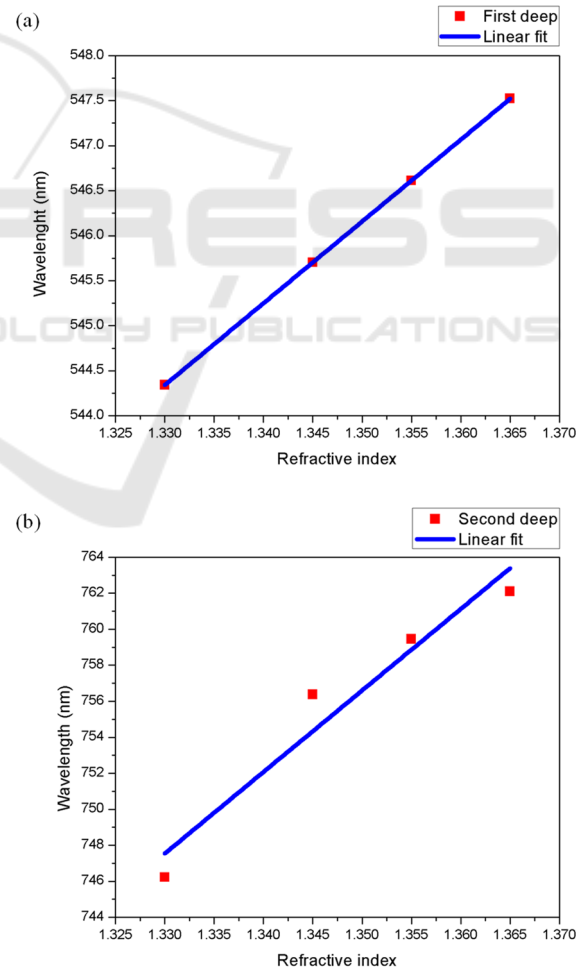s in exploring the sensitivity of the first and second peaks, corresponding to single and aggregated nanoparticles, respectively. The sensitivity to the surrounding refractive index was found to be 90 nm/RIU for the first peak and 4 times higher, at 450 nm/RIU, for the second peak. This sensor holds promise for applications in sensing chemical concentrations based on changes in the surrounding refractive index around nanoparticles.

REFERENCES

Bastús, N. G., Comenge, J., & Puntes, V. (2011). Kinetically Controlled Seeded Growth Synthesis of Citrate-Stabilized Gold Nanoparticles of up to 200 nm: Size Focusing versus Ostwald Ripening. *Langmuir*, *27*(17), 11098–11105. https://doi.org/10.1021/la201938u

Chau, L.-K., Lin, Y.-F., Cheng, S.-F., & Lin, T.-J. (2006). Fiber-optic chemical and biochemical probes based on localized surface plasmon resonance. *Sensors and Actuators B: Chemical*, *113*(1), 100–105. https://doi.org/10.1016/j.snb.2005.02.034

Choudhary, S., Esposito, F., Sansone, L., Giordano, M., Campopiano, S., & Iadicicco, A. (2023). Lossy Mode Resonance Sensors in Uncoated Optical Fiber. *IEEE Sensors Journal*, *23*(14), 15607–15613. https://doi.org/10.1109/JSEN.2023.3280675

Do, P. Q. T., Huong, V. T., Phuong, N. T. T., Nguyen, T.-H., Ta, H. K. T., Ju, H., Phan, T. B., Phung, V.-D., Trinh, K. T. L., & Tran, N. H. T. (2020). The highly sensitive determination of serotonin by using gold nanoparticles (Au NPs) with a localized surface plasmon resonance (LSPR) absorption wavelength in the visible region. *RSC Advances*, *10*(51), 30858–30869. https://doi.org/10.1039/D0RA05271J

Esfahani Monfared, Y. (2020). Overview of Recent Advances in the Design of Plasmonic Fiber-Optic Biosensors. *Biosensors*, *10*(7), 77. https://doi.org/10.3390/bios10070077

Esposito, F., Srivastava, A., Sansone, L., Giordano, M., Campopiano, S., & Iadicicco, A. (2021). Label-Free Biosensors Based on Long Period Fiber Gratings: A Review. *IEEE Sensors Journal*, *21*(11), 12692–12705. https://doi.org/10.1109/JSEN.2020.3025488

Guerreiro, J. R. L., Frederiksen, M., Bochenkov, V. E., De Freitas, V., Ferreira Sales, M. G., & Sutherland, D. S. (2014). Multifunctional Biosensor Based on Localized Surface Plasmon Resonance for Monitoring Small Molecule–Protein Interaction. *ACS Nano*, *8*(8), 7958–7967. https://doi.org/10.1021/nn501962y

Hernandez-Romano, I., Monzon-Hernandez, D., Moreno-Hernandez, C., Moreno-Hernandez, D., & Villatoro, J. (2015). Highly Sensitive Temperature Sensor Based on a Polymer-Coated Microfiber Interferometer. *IEEE Photonics Technology Letters*, *27*(24), 2591–2594. https://doi.org/10.1109/LPT.2015.2478790

Huong, V. T., Phuong, N. T. T., Tai, N. T., An, N. T., Lam, V. D., Manh, D. H., Chi, T. T. K., Mai, N. X. D., Phung, V.-D., & Tran, N. H. T. (2021). Gold Nanoparticles Modified a Multimode Clad-Free Fiber for Ultrasensitive Detection of Bovine Serum Albumin. *Journal of Nanomaterials*, *2021*, 1–6. https://doi.org/10.1155/2021/5530709

Jain, P. K., Lee, K. S., El-Sayed, I. H., & El-Sayed, M. A. (2006). Calculated Absorption and Scattering Properties of Gold Nanoparticles of Different Size, Shape, and Composition: Applications in Biological Imaging and Biomedicine. *The Journal of Physical Chemistry B*, *110*(14), 7238–7248. https://doi.org/10.1021/jp0571700

Lei, H., Zhu, S., Liu, C., Zhang, W., Chen, C., & Yan, H. (2023). Constructing the Au nanoparticle multimer on optical fiber end face to enhance the signal of localized surface plasmon resonance biosensors: A case study for deoxynivalenol detection. *Sensors and Actuators B: Chemical*, *380*, 133380. https://doi.org/10.1016/j.snb.2023.133380

Litti, L., & Meneghetti, M. (2019). Predictions on the SERS enhancement factor of gold nanosphere aggregate samples. *Physical Chemistry Chemical Physics*, *21*(28), 15515–15522. https://doi.org/10.1039/C9CP02015B

Lu, J., Yu, Y., Qin, S., Li, M., Bian, Q., Lu, Y., Hu, X., Yang, J., Meng, Z., & Zhang, Z. (2022). High-performance temperature and pressure dual-parameter sensor based on a polymer-coated tapered optical fiber. *Optics Express*, *30*(6), 9714. https://doi.org/10.1364/OE.452355

Mayer, K. M., & Hafner, J. H. (2011). Localized Surface Plasmon Resonance Sensors. *Chemical Reviews*, *111*(6), 3828–3857. https://doi.org/10.1021/cr100313v

Saha, K., Agasti, S. S., Kim, C., Li, X., & Rotello, V. M. (2012). Gold Nanoparticles in Chemical and Biological Sensing. *Chemical Reviews*, *112*(5), 2739–2779. https://doi.org/10.1021/cr2001178

Sansone, L., Campopiano, S., Pannico, M., Giordano, M., Musto, P., & Iadicicco, A. (2021). Photonic bandgap influence on the SERS effect in metal-dielectric colloidal crystals optical fiber probe. *Sensors and Actuators B: Chemical*, *345*, 130149. https://doi.org/10.1016/j.snb.2021.130149

Soares, M. S., Vidal, M., Santos, N. F., Costa, F. M., Marques, C., Pereira, S. O., & Leitão, C. (2021a). Immunosensing Based on Optical Fiber Technology: Recent Advances. *Biosensors*, *11*(9), 305. https://doi.org/10.3390/bios11090305

Soares, M. S., Vidal, M., Santos, N. F., Costa, F. M., Marques, C., Pereira, S. O., & Leitão, C. (2021b).

Immunosensing Based on Optical Fiber Technology: Recent Advances. *Biosensors*, *11*(9), 305. https://doi.org/10.3390/bios11090305

Sypabekova, M., Hagemann, A., Rho, D., & Kim, S. (2022). Review: 3-Aminopropyltriethoxysilane (APTES) Deposition Methods on Oxide Surfaces in Solution and Vapor Phases for Biosensing Applications. *Biosensors*, *13*(1), 36. https://doi.org/10.3390/bios13010036

Unser, S., Bruzas, I., He, J., & Sagle, L. (2015). Localized Surface Plasmon Resonance Biosensing: Current Challenges and Approaches. *Sensors*, *15*(7), 15684–15716. https://doi.org/10.3390/s150715684

Wang, Y., Zhou, J., & Li, J. (2017). Construction of Plasmonic Nano-Biosensor-Based Devices for Point-of-Care Testing. *Small Methods*, *1*(11). https://doi.org/10.1002/smtd.201700197

Willets, K. A., & Van Duyne, R. P. (2007). Localized Surface Plasmon Resonance Spectroscopy and Sensing. *Annual Review of Physical Chemistry*, *58*(1), 267–297. https://doi.org/10.1146/annurev.physchem.58.032806.104607

Zeng, S., Yong, K.-T., Roy, I., Dinh, X.-Q., Yu, X., & Luan, F. (2011). A Review on Functionalized Gold Nanoparticles for Biosensing Applications. *Plasmonics*, *6*(3), 491–506. https://doi.org/10.1007/s11468-011-9228-1